Article

J. Biol. Regul. Homeost. Agents. 2024; 38(5): 4465–4476
https://doi.org/10.23812/j.biol.regul.homeost.agents.20243805.355

Unveiling Berberine's Potential for Hepatocellular Carcinoma: Empowered by Molecular Docking-Driven Nanoparticle Enhancement

Gehan A. M. Khodear[1], Muhammad Alaa Eldeen[2,*], Waleed K. Abdulsahib[3], Samy A. Dawood[4], Mohammed A. Alshehri[4], Tarig Gasim M. Alarabi[5], Aymen Nasreldin A. Mohammed[6], Ashraf K. Awaad[7], Refaat A Eid[8], Mohamed A Akl[9,10], Mohamed Samir A. Zaki[5], Nievin Ahmed Mahran[11]

[1]Medical Technology Center, Medical Research Institute, Alexandria University, 5424041 Alexandria, Egypt
[2]Cell Biology, Histology, & Genetics Division, Zoology Department, Faculty of Science, Zagazig University, 7120001 Alsharquia, Egypt
[3]Department of Pharmacology and Toxicology, College of Pharmacy, Al-Farahidi University, 00965 Baghdad, Iraq
[4]Department of Child Health, College of Medicine, King Khalid University, 62529 Abha, Saudi Arabia
[5]Department of Anatomy, College of Medicine, King Khalid University, 61421 Abha, Saudi Arabia
[6]Department of Anatomy, Faculty of Medicine, Najran University, 66454 Najran, Saudi Arabia
[7]Center of Excellence for Research in Regenerative Medicine and its Applications (CERRMA), Faculty of Medicine, Alexandria University, 5424041 Alexandria, Egypt
[8]Department of Pathology, College of Medicine, King Khalid University, 12573 Abha, Saudi Arabia
[9]Department of Pharmaceutics and Pharmaceutical Technology, Faculty of Pharmacy (Boys), Al-Azhar University, 4434003 Cairo, Egypt
[10]Department of Pharmaceutics, College of Pharmacy, The Islamic University, 54001 Najaf, Iraq
[11]Department of Biochemistry, Faculty of Dentistry, Sinai University, 16020 Kantara, Egypt
*Correspondence: dr.muhammadalaa@gmail.com (Muhammad Alaa Eldeen)
Published: 1 May 2024

Background: Hepatocellular carcinoma (HCC) poses a significant challenge in oncology due to its high mortality rates and limited treatment options resulting from its aggressive nature and often late-stage diagnosis.
Objective: This study aimed to systematically identify a potent anti-HCC agent to address the challenges.
Materials and Methods: Initiating with a molecular docking analysis, a comprehensive virtual screening of various compounds was conducted to identify the most promising anti-HCC agent. Berberine (BBR), an isoquinoline alkaloid derived from *Hydrastis canadensis* and *Coptis chinensis*, emerged as the most potent candidate, showcasing diverse anti-cancer mechanisms. The BBR, historically recognized for managing bacterial diarrhea, faces challenges in clinical application against HCC due to limitations in solubility and bioavailability. To overcome these constraints, this study employed a protein-based nanoparticulate drug delivery system, leveraging bovine serum albumin nanoparticle (BSA NP) advantages. The synthesis of BSA NPs encapsulating BBR was meticulously executed, yielding BBR-BSA NPs.
Results: Subsequent *in vitro* investigations unequivocally demonstrated the heightened cytotoxicity of BBR when encapsulated within BSA NPs, showcasing superior efficacy compared to free BBR. These nanoformulations exhibited pronounced induction of apoptosis in hepatoma cells, highlighting their enhanced therapeutic potential.
Conclusions: In conclusion, this comprehensive approach not only reveals the promise of BBR-BSA NPs in combatting human hepatoma but also represents a significant advancement by addressing limitations associated with conventional BBR formulations, offering improved solubility and bioavailability in the context of HCC therapy.

Keywords: Berberine; docking; hepatocellular carcinoma; bovine; nanoparticles

Introduction

Hepatocellular carcinoma (HCC) represents a prevalent human cancer, representing the second most frequent contributor to cancer-related mortalities [1]. Accordingly, a new therapeutic agent of natural origin with outstanding effectiveness and an innovative strategic delivery system that leads to low toxicity and remarkable selectivity needs further research. Berberine (BBR), the natural isoquinoline alkaloid compound, is obtained through the Berberis genus's roots, rhizomes, and stem bark. In Chinese and Ayurvedic medicine, BBR plant extracts have been utilized for many years [2]. Particularly, BBR has been elucidated to possess several pharmacological activities on inflammation [3], reactive oxygen species (ROS) [4], diabetes [5], hyperten-

Copyright: © 2024 The Author(s). Published by Biolife Sas. This is an open access article under the CC BY 4.0 license.
Note: *J. Biol. Regul. Homeost. Agents.* stays neutral with regard to jurisdictional claims in published maps and institutional affiliations.

Journal of
BIOLOGICAL REGULATORS
and Homeostatic Agents

sion [6], depression [7], microbes [8,9], neuro diseases [10], hepatic disorders [11], and hyperlipidemia [12], as well as have anti-cancer efficacy [13,14]. Although BBR has been revealed to exert an anti-cancer impact by modulating various proapoptotic, antiapoptotic, and intrinsic pathways [15–17], its key limitations include low bioavailability, inadequate water solubility, and constrained absorption in the digestive system [18]. This restricts its applicability and results in low effective concentrations at the action site.

Biodegradable delivery vehicles provide an absolute answer to each of these drug delivery issues. As a powerful drug delivery vehicle, protein biomolecules have lately emerged as an option to overcome the constraints of conventional treatments that included poor water solubility, low bioavailability, and unsatisfactory therapeutic effects. Because of the tumor's immature, high permeability, and leaky vasculature, protein-based delivery systems, such as albumin, naturally accumulate within the tumor site and exhibit improved permeability as well as retention impact [19].

The therapeutic applications of nanoparticles (NPs) relying upon bovine serum albumin (BSA)/human serum albumin have been thoroughly explored. These NPs are abundant in blood, convenient to purify, non-toxic, biodegradable, and low in immunogenicity, besides having a high accumulation at tumor sites and biocompatibility, rendering them an optimum candidate for NP synthesis [20].

Recently, many albumin-based medicines and imaging agents have been created and are available on the market, and several clinical trials are being conducted for various purposes [21,22]. Therefore, BSA has become a popular nano-drug carrier in various clinical applications in light of these considerations. Albumin, a prevalent plasma protein having a 66.5 kDa molecular weight, sustains plasma colloidal osmotic pressure, transports nutrients to various cell areas, and stabilizes the blood pH. Moreover, it has an unusual capacity to solubilize hydrophobic fatty acid molecules and is extremely stable throughout a pH of 4–9 [23]. Because of its ability to transport hydrophobic medicines in an aqueous solution, BSA improves the pharmacokinetics of the bound ligands in a physiological environment [24]. Accordingly, our study selected BSA as the preferred nanocarrier for BBR to optimize drug delivery efficiency. The potential of nanoparticulate polymeric drug delivery systems using BBR to treat liver cancer has yet to be investigated. Consequently, we aimed to evaluate the efficacy of employing BSA as a non-toxic, biodegradable, and biocompatible protein as a nanoparticulate drug delivery system in increasing BBR solubility and bioavailability to enhance its anti-cancer activity. This was performed to prevent proteolytic degradation of the active ingredient BBR by BSA as a delivery vehicle and enables a longer time in the bloodstream.

Materials and Methods

Materials

Herein, BSA 96% and BBR 95% were procured from Sigma-Aldrich (Patch No. 9048-46-8 and 633-66-9, St. Louis, MO, USA) while obtaining the human hepatoma cell line (HepG2) from the Cell Culture Department of VACSERA (Cairo, Egypt). Prior to experimentation, we validated the cell line identity through Short Tandem Repeat analysis, and mycoplasma contamination was assessed using appropriate detection methods, revealing negative results. The cells went through culture at 37 °C in a 5% CO_2 humidified incubator for 24 h. Our study conducted all experiments in polypropylene flasks suitable for cell culture.

Methods

Molecular Docking Study

Receptors and ligand retrieval for docking study BBR (PubChem CID: 2353) 3D conformer was downloaded to act as a ligand through https://pubchem.ncbi.nlm.nih.gov/compound/berberine. Investigating the literature on the mechanism of action of BBR identified six main target proteins for the docking study [25–27]. These proteins were alpha serine/threonine-protein kinase (AKT1; PDB ID: 3MV5), caspase-3 (PDB ID: 3KJF), epidermal growth factor receptor (EGFR; PDB ID: 4I23), extracellular signal-regulated kinase 2 (ERK-2; PDB ID: 4ZZM), P38 (PDB ID: 3U8W), and signal transducer and activator of transcription 3 (STAT3; PDB ID: 6NJS). The target receptors were first prepared by removing water and adding polar hydrogens and Kollman charges. The deposited molecule in each receptor was then removed and saved to serve as a control for validating the BBR docking scores. The docking analysis was conducted through AutoDock Vina (Version 1.1.2, The Scripps Research Institute, La Jolla, CA, USA) [28], and the result was visualized through the molecular graphics system PyMOL (Version 2.4.1, Schrödinger, LLC, New York, NY, USA) [29].

Synthesizing Bovine Serum Albumin Nanoparticles (BSA NPs) and BBR-BSA NPs

Our study synthesized BSA NPs and BBR-BSA NPs with minor modifications through the desolvation procedure reported early by Solanki *et al.* [30]. The BSA NPs were prepared by dissolving 200 mg of BSA in 2 mL of Milli-Q (MQ) water, followed by 10-min incubation at room temperature (RT; 25 °C) under stirring at 500 rpm. Subsequently, we dropwisely added 8 mL of ethanol (1 mL/min) to the pre-prepared BSA solution at RT while stirring continuously (500 rpm) until the solution appeared milky. The solution was cross-linked with 235 µL of glutaraldehyde (8% v/v) (Patch No.111-30-8, Thermo Fisher Scientific, Waltham, MA, USA) with continuing stirring for 24 h to stabilize the process. The resultant NPs were purified using 3 centrifugation cycles at 10,000 rpm for 10

min, subsequent by redispersion within 1 mL of MQ water and 5-min sonication at RT. Before being lyophilized, the solution was held overnight at 80 °C. Additionally, we prepared BBR-BSA NPs by dissolving 20 mg of BBR in 8 mL of 100% ethanol. Subsequently, we used 2 mL of MQ water to dissolve 200 mg of BSA, which was then treated with 1 M NaOH solution to raise the pH to 7.4. Afterward, the BSA solution was gradually infused with the BBR solution while stirring continuously (1 mL/min; 500 rpm). The remaining processes were identical to those used in synthesizing BSA NPs. Eventually, BSA NPs and BBR-BSA NPs went through lyophilization and were kept at 4 °C for subsequent usage.

Characterizing NPs

The Zetasizer (NanoS90, Malvern Panalytical, Malvern, UK) was used to detect the hydrodynamic particle size distribution utilizing dynamic light scattering (DLS) at 25 °C. Our study examined the lyophilized BSA NPs and BBR-BSA NPs for shape and size. Transmission electron microscopy (TEM; JEOL-100 CX, JEOL Ltd., Tokyo, Japan) was utilized at 10 kV acceleration voltage. The samples underwent sonication employing a bath sonicator for 10 min, aiming at dispersing the NPs. Then, 10 µL of each sample was loaded onto a 300-mesh copper grid coated with carbon film (Patch No. NC0205992, Ted Pella, Inc., Redding, CA, USA) and allowed to dry in the air. Grids containing the samples were negatively stained using 2% uranyl acetate (Patch No. 6159-44-0, Ted Pella, Inc., Redding, CA, USA), dried at RT, and examined using TEM. A fourier-transform infrared spectrophotometer (Nicolet iS50 FTIR, Thermo Scientific, Waltham, MA, USA) was employed to analyze fourier-transform infrared spectroscopy (FTIR) spectra of pure BBR, BSA NPs, and BBR-BSA NPs in a 4000–400 cm^{-1} range.

Encapsulation Efficiency (EE)

The apparent EE of BBR amount in BBR-BSA NPs was determined indirectly. Briefly, a 2 mL aliquot of BBR-BSA NPs was ultra-centrifuged for 3 h at 10,000 rpm and 4 °C through a Beckman Optima™ Ultracentrifuge (Optima™ XL, Beckman Coulter, Inc, Indianapolis, IN, USA). Free unencapsulated BBR proportion was spectrophotometrically analyzed (UV-1800 PC, Shimadzu, Kyoto, Japan) at 343 nm against blank. The apparent EE% was then calculated using the following equation:

$$\mathbf{EE\%} = \left[\frac{\textbf{Total BBR–BSA–NPs amount–Free BBR}}{\textbf{Total BBR–BSA–NPs amount}} \times 100\right] \quad (1)$$

Cell Culture Study

The HepG2 cell line was utilized to conduct *in vitro* cell culture and cytotoxicity analysis on the pre-synthesized BBR-BSA NPs. The cells were kept alive by utilizing Dulbecco's Modified Eagle Medium/Nutrient Mixture F-12 (DMEM/F12) (Patch No.10565, Thermo Fisher Scientific, Waltham, MA, USA) media containing 10% fetal bovine serum (Patch No. F2442) and 100 U/mL of streptomycin/penicillin (Patch No. P4458, both from Sigma-Aldrich, St. Louis, MO, USA) in a 5% CO_2 incubator at 37 °C. Herein, 3×10^3 cells were placed in each well of 96-well plates and subjected to overnight incubation at 37 °C with humified 5% CO_2 and 95% air until a subconfluent state of 1×10^4 cells per well was reached.

Cell Viability Assay

Cell viability was conducted by employing a 3-(4,5-dimethylthiazol-2-yl)-2,5-diphenyltetrazolium bromide assay (MTT; Patch No. 475989, Sigma-Aldrich, St. Louis, MO, USA) to evaluate BBR influence on HepG2 cell line growth. This colorimetric test depends on the selective capacity of the live cells to decrease the tetrazolium component of MTT to purple formazan crystals. In brief, 5×10^3 cells/well were seeded in 96-well plates overnight and went through 37 °C incubation at a humidified 5% CO_2 incubator. Subsequently, the cells were incubated with BBR, BSA, and BBR-BSA NPs over 72 h by substituting the older media with new media comprising various BBR concentrations and formulations (1, 2.5, 5, 10, 20, and 50 µm/mL). Untreated control wells were subjected to seeding with cells incubated without BBR, BSA, or BBR-BSA NPs.

After 72 h incubation, cells were gently rinsed two times in a 96-well microplate with phosphate buffer saline (PBS; Patch No. 79382, Sigma-Aldrich, St. Louis, MO, USA). Our study evaluated cell viability by adding 1 mM of MTT to the cells incubated for 4 h at 37 °C. Cell supernatant was subsequently eliminated, dissolving formazan precipitates in 100 µL dimethyl sulfoxide (DMSO; Patch No. 20-139, Sigma-Aldrich, St. Louis, MO, USA), followed by 15-min re-incubation.

Next, the MTT formazan crystals were allowed to dissolve by adding DMSO and then incubated again for 10 min, measuring the absorbance values at 570 nm through an automated microplate reader (Wallac 1420 Victor2, Wallac Oy, Turku, Finland). The absorbance for background adjustment was determined at 620 nm. The blank for measuring absorbance was obtained by filling wells with medium alone. The cell survival percentage was determined by applying the formula below after adjusting for background absorbance and subtracting the blank absorbance:

$$\text{Cell viability (\%)} = \frac{\textbf{Mean optical density of treated wells}}{\textbf{Mean optical density of control wells}} \times 100 \quad (2)$$

Cellular Uptake Study

The BBR and BBR-BSA NP uptake was visualized with confocal laser scanning microscopy (CLSM, Leica TSC SPE II/DMi 8, Wetzlar, Germany). The following wavelengths were employed for fluorescence detection: 488 and 405 nm for BBR (autofluorescence) and the

Journal of
BIOLOGICAL REGULATORS
and Homeostatic Agents

nuclei-staining dye, respectively. The photomicrographs were morphometrically analyzed using mean area percent (MA%) and mean fluorescence intensity through image analysis software (Version 1.52p; Image J; 1.52p software 32, NIH, Bethesda, MD, USA). The HepG2 cell (0.5×10^5 cells/well) seeding was performed into a UV-disinfected 6-well plate with covered glass and incubated overnight and followed by BBR and BBR-BSA NP treatment for 4 and 24 h at 37 °C in a CO_2 incubator. After that, we removed the medium and rinsed the cells gently three times using PBS. Then, the cells went through fixation utilizing 4% paraformaldehyde for 10 min at RT and a three-time wash utilizing PBS to remove paraformaldehyde. The cells were then permeabilized using 0.1% Triton X-100 (Patch No. HFH10, Thermo Fisher Scientific, Waltham, MA, USA) for 10 min at RT and rinsed with PBS three times to remove the Triton X-100. Therefore, the nuclei were stained utilizing 4′,6-diamidino-2-phenylindole (DAPI; Patch No. 28718-90-3, Sigma-Aldrich, St. Louis, MO, USA) dissolved in VECTASHIELD Antifade Mounting Medium (H-1000-10, Vector Laboratories, Burlingame, CA, USA).

Assessment of Lactate Dehydrogenase (LDH), Caspase-3 Activity, and Reduced Glutathione (GSH) Concentration in Treated HepG2 Cells

The LDH activity in the cell medium was evaluated using kits obtained from Bio-Systems S.A. (Patch No. MAK066) per the protocols. The HepG2 cells (0.5×10^6 cells/well) were seeded in 6-well plates and treated with paclitaxel IC_{50} (Patch No. 33069-62-4), liposomal paclitaxel, and epigallocatechin gallate (EGCG; Patch No. 989-51-5; 50 µM) in combination with liposomal paclitaxel. The kits and reagents are all sourced from Sigma-Aldrich, St. Louis, MO, USA. After 72-h incubation at CO_2, the media were gathered for LDH activity assessment. For LDH activity assessment, we introduced 10 µL of the treated cell medium to 500 µL of working reagent. Initial absorbance was recorded after 30 s, followed by measurements at 1-min intervals for 3 min. The average absorbance difference/min (ΔA/min) was calculated from consecutive absorbance differences. The LDH activity (U/L) was computed using the formula: $\Delta A/\text{min} \times (Vt \times 106) / (\varepsilon \times l \times Vs) = U/L$. Here, the total reaction volume (Vt) was 0.510, the molar absorbance (ε) of NADH at 340 nm was 6300, the light path (l) was 1 cm, the sample volume (Vs) was 0.010, and 1 U/L equated to 0.0166 µkat/L. This experiment employed HepG2 cells to assess LDH activity post-treatment with different agents. Appropriate controls were included to ensure comparative analysis alongside the treated samples.

The HepG2 cells (0.5×10^6 cells/well) were plated in 6-well plates, subjected to treatment with 20 ug/mL of BBR, BSA NPs, and BBR-BSA NPs, and cultured for 72 h in a CO_2 incubator. Eventually, our study lysed the cell pellet by centrifugation at 3000 rpm, aiming at assessing caspase-3 activity and reduced GSH levels.

Caspase-3 activity was determined in culture supernatants by employing the caspase-3 ELISA kit (Patch No. BMS2012INST, Thermo Fisher Scientific, Waltham, MA, USA). The quantitative sandwich enzyme immunoassay method was used following Nicholson, 1997 [31]. A 96-well microplate was coated in advance with a monoclonal antibody that specifically targets caspase-3. The standards and unknown samples were added to the wells, where the immobilized antibody captured any caspase-3 present. Following rinsing, a substrate solution was introduced, and the resultant color was directly proportional to the quantity of caspase-3 bound in the first step. The optical density and color intensity values were then measured spectrophotometrically by a microplate reader (Infinite F50, Tecan, Männedorf, Switzerland) at 450 nm. The GSH levels in cell lysate were assessed through the technique reported by Beutler *et al.* (1963) [32]. Briefly, 2-nitro-5-thiobenzoic acid (TNB) was formed by reducing 5,5′-dithio-bis-(2-nitrobenzoic acid) (DNTB; Patch No. 22582, Thermo Fisher Scientific, Waltham, MA, USA) with GSH. After resuspending the cell pellet in the lysis buffer, we centrifuged the homogenate for 5 min at 4000 rpm and 4 °C, collecting the supernatant for analysis. A 50 µL aliquot of the supernatant was combined with 1.7 mL of 0.3 M disodium hydrogen phosphate (Na_2HPO_4; Patch No. 7558-79-4, Sigma-Aldrich, St. Louis, MO, USA) and 250 µL of DNTB reagent. The resultant yellow-colored product TNB was measured spectrophotometrically at 412 nm (Photometer 5010 V5+, WTW, Weilheim, Germany). The GSH levels were assessed via a standard reduced GSH curve and expressed in micromoles/mg of protein.

DNA Fragmentation Assay

DNA fragmentation was conducted following Rahbar *et al.* (2015) [33]. Briefly, DNA extraction was performed from treated HepG2 cells through Quick-gDNA™ MiniPrep Kit (Zymo Research D3024, Zymo Research Corp., Irvine, CA, USA). Isolated DNA purity and concentration were assessed via a NanoDrop 2000 spectrophotometer (Thermo Fischer Scientific, Waltham, MA, USA). Moreover, DNA electrophoresis was carried out on 1% agarose gel and stained utilizing 0.5 µg/mL ethidium bromide (Patch No. 1239-45-8, Sigma-Aldrich, St. Louis, MO, USA). Non-fragmented DNA had a smear form; however, after treatment, fragmented DNA appeared at a varied distance from the cathode on the gel sheet, depending on its base pairs [34].

Statistical Analysis

Statistical analyses were conducted through the SPSS 20.0 software package (IBM Corp., Armonk, NY, USA), reporting the data as mean ± standard deviation (SD). Differences in LDH, caspase-3, reduced GSH relative levels, and DNA fragmentation were analyzed employing the ANOVA test. $p < 0.05$ indicated statistical significance.

Table 1. The generated binding energy of Berberine (BBR) and the control with target proteins.

Target	Control binding energy	BBR binding energy	BBR interacting residues
AKT-1	–7.9	–9.0	ARG4, LYS158, LYS179, PHE161, SER7, LEU252, HIS194, GLU198, and THR195
Caspase-3	–8.1	–7.6	HIS121, TRP206, GLN161, ARG64, and ARG207
EGFR	–8.2	–8.7	LYS745, LEU788, ALA743, THR790, LEU718, LEU792, MET793, and GLY796
ERK-2	–7	–7.4	ASP167, LEU156, LEU107, GLY34, LYS54, VAL39, and MET108
P38	–11.8	–8.4	THR106, ASP168, LEU75, and LEU167
STAT-3	–8.1	–7.4	ARG335, MET470, ILE569, and ASP570

Control: a blank nanoparticle (free from BBR). AKT-1, serine/threonine-protein kinase 1; EGFR, epidermal growth factor receptor; ERK-2, extracellular signal-regulated kinase 2; STAT-3, signal transducer and activator of transcription 3.

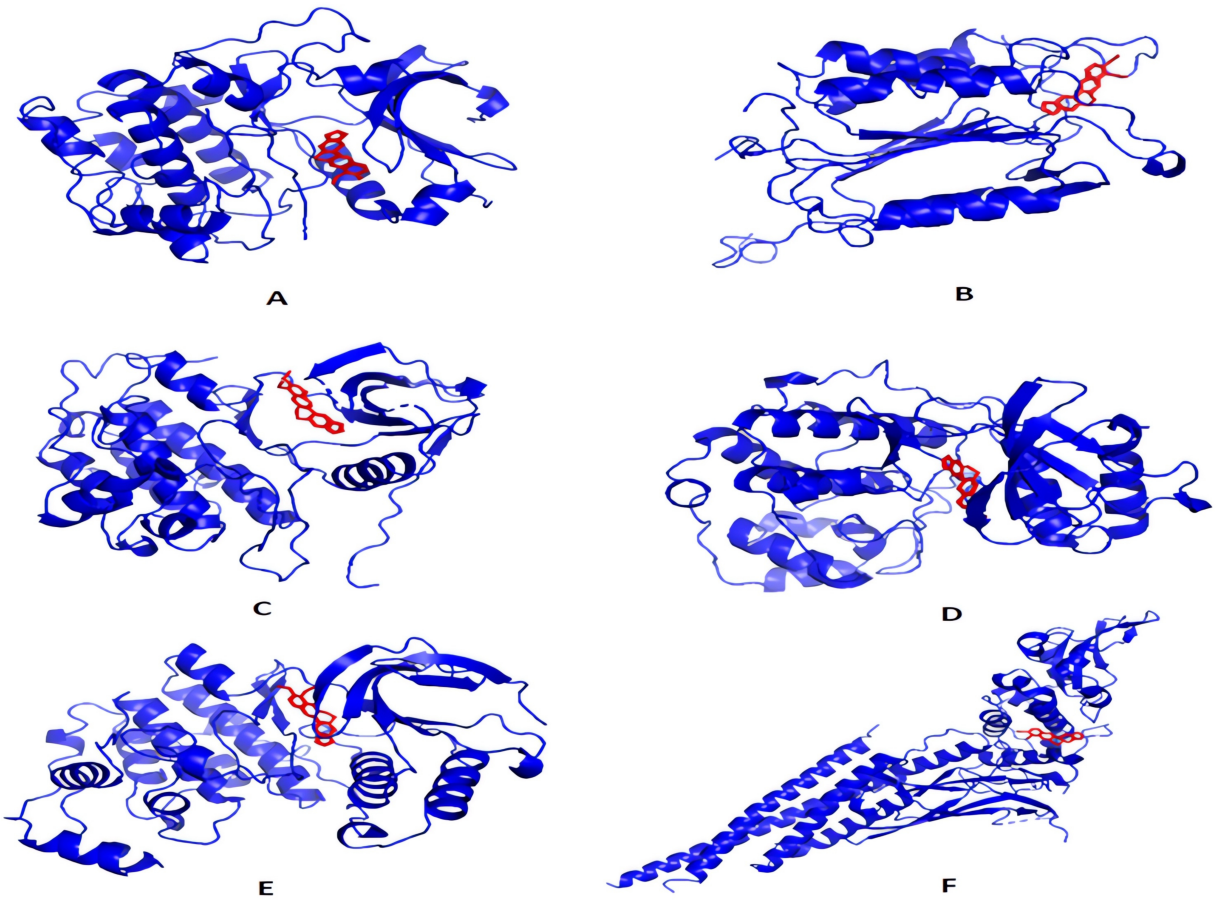

Fig. 1. Interaction sites: visualization of BBR binding with key proteins. Docking site of BBR with (A) AKT-1, (B) Caspase-3, (C) EGFR, (D) ERK-2, (E) P38, and (F) STAT-3, where BBR is in red and target protein is in blue.

Results

BBR Docking with its Targets

The docking study was performed two times per receptor (one for BBR and one for control), showing the binding energy for each docked complex in Table 1. Comparison of the generated binding scores of BBR and control docked complexes revealed proximity in the binding values, which supports the literature that selected proteins as targets for the BBR effect as an anti-tumor agent. The binding energy of BBR with serine/threonine-protein kinase 1 (AKT-1), EGFR, and ERK-2 was greater (more negative) than the control's, indicating stronger binding affinity. Fig. 1 depicts the location of docked BBR in each of the six proteins, and Table 1 lists the interacting residues.

BSA NP and BBR-BSA NP Synthesis and Characterizations

Zeta Potential (ZP)

Desolvation (or coacervation) methods successfully prepared BBR-BSA NPs' formulation. The NPs were evaluated for ZP (Fig. 2A), indicating that the ZP of BSA NP

Journal of
BIOLOGICAL REGULATORS
and Homeostatic Agents

formulation exhibited a negatively charged value of –1.45 mV, which, after BBR loading, the medicated formulation (BBR-BSA NPs) displayed a high negative value of –15.3 mV (Fig. 2B).

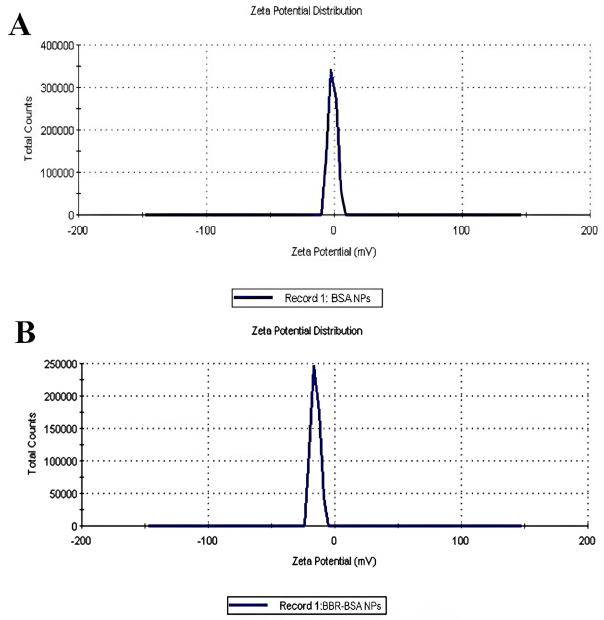

Fig. 2. Comparative Zeta potential of BSA and Berberine-bovine serum albumin (BSA) Nanoparticles. Zeta potential distribution graphs of (A) Bovine serum albumin nanoparticles (BSA NPs) and (B) Berberine-BSA NPs (BBR-BSA NPs) determined through dynamic light scattering.

FTIR

FTIR spectroscopy was employed to verify the BBR-BSA NP production, representing the BSA NP and BBR-BSA NP characteristic spectrum in Fig. 3. The FTIR spectrum of BSA NPs (line I) revealed absorption characteristic bands at 2977.51 and 2838.84 cm^{-1} representing C–H stretching (alkanes), 1086.7 cm^{-1} for ring deformation and C-H in-plane bending, 1032.5 cm^{-1} for C–H vibrations, and 1452.81 cm^{-1} for aromatic C=C vibrations in the aromatic ring [35]. The FTIR spectrum of BBR-BSA NPs (line II) demonstrated the basic characteristic peaks of the protein, serum albumin (SA) structure, and BSA NPs without any significant change. However, it shifted to higher frequencies at 3386.5 (amide A, correlated with N–H stretching), 2978.75 (amide B, N–H stretching of NH_3^+ free ion), 1640.10 (amide I, C=O stretching), 1452.97 (amide II, related to C–N stretching and N–H bending vibrations), and nearly 1406.38 cm^{-1} (CH2 bending groups) [36]. A protein structure was assessed utilizing amide I/II/III and IR absorption peaks [37]. Ultimately, the findings indicate BBR-BSA NP synthesis.

Encapsulation Efficiency

The EE% of BBR-BSA NPs was determined to be 77.82 ± 2.031%. This value indicates the proportion of Berberine successfully encapsulated within the bovine serum albumin nanoparticles. The high EE% suggests effective loading of the drug into the nanoparticles.

Morphology of BSA NPs and BBR-BSA NPs

The TEM results (Fig. 4A,B) revealed that BSA NPs and BBR-BSA NPs have nanostructures with a spherical shape, with sizes of about 15.458 ± 1.42 and 36.66 ± 0.97 nm, respectively.

In Vitro HepG2 Cell Viability

The HepG2 cell proliferation was evaluated employing an MTT assay over 72 h, demonstrating that BBR, BSA, and BBR-BSA NPs inhibited HepG2 cell proliferation dose-dependently (Fig. 5). Moreover, BBR-BSA NPs (10.3 µg/mL) and BBR (15.58 µg/mL) gave 50% toxicity for HepG2 cells, whereas 25.43 µg/mL of BSA NPs were required for 50% toxicity toward HepG2 cells.

Cellular Uptake and Localization of BSA NPs, BBR, and BBR-BSA NPs in HepG2 Cells

The CLSM findings depicted that BSA NPs had nearly no detectable fluoresce after 4 or 24 h of incubation (Fig. 6). The HepG2 cell lines could take up BBR and BBR-BSA NPs at various capacities, where both appeared as bright green fluorescence in the cytoplasm, revealing their successful internalization in HepG2 cells. The BBR-BSA NP fluorescence intensity was stronger than BBR after 4 h incubation. Furthermore, intracellular fluorescence intensity was enhanced with time, after 24 h incubation, demonstrating that BBR and BBR-BSA NP cellular internalization was time-dependent. The BBR-BSA NP fluorescence intensity following 24 h incubation was significantly higher than BBR-BSA NPs after 4 h incubation.

Apoptosis Assay

The apoptotic effects were measured using LDH, caspase-3, reduced GSH, and DNA fragmentation (Table 2). The LDH concentration (U/L) measurements in treated HepG2 cells with BSA NPs, BBR free, and BBR-BSA NPs were 82.3, 85.1, and 101.7 U/L respectively, revealing that treated cells significantly increased LDH in comparison to the untreated control cell (Table 2; $p < 0.001$). The BBR-BSA NP treatment significantly increased the content of caspase-3 level by about 3.5-fold in treated cells (7.03 ng/mL) compared to the untreated cells (2.01 ng/mL; $p < 0.001$). When HepG2 cells were treated with 15.58, 25.43, and 10.3 µg/mL of BBR, BSA NPs, and BBR-BSA NPs for 72 h, the GSH level in treated HepG2 cells with BBR-BSA NPs was significantly higher (83.1 µmol/mg) than untreated controls (35.2 µmol/mL) or treated with BBR free solution (62.5 µmol/mL) of BSA NPs

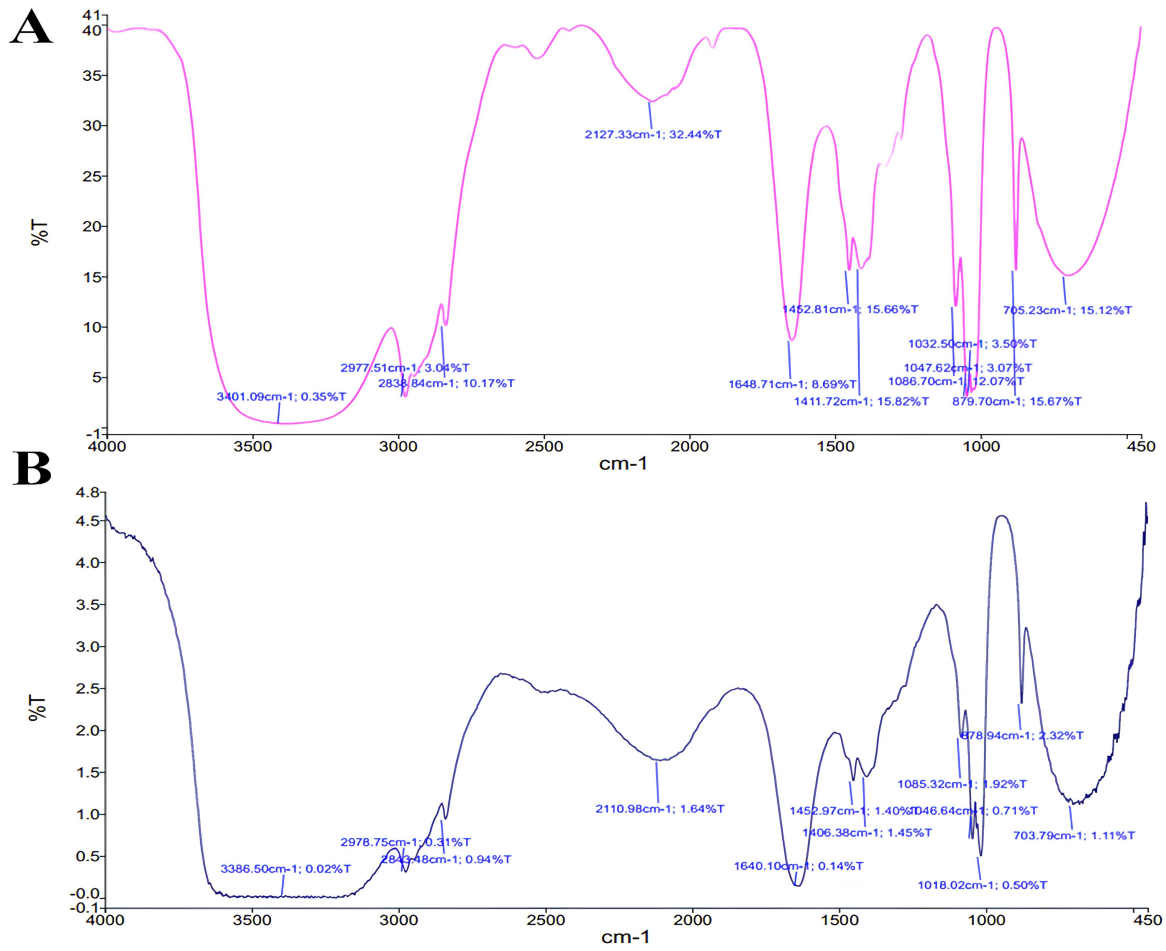

Fig. 3. Fourier-transform infrared spectroscopy (FTIR) spectral analysis of BSA and Berberine-BSA nanoparticles. The fourier-transform infrared spectrophotometer spectra of BSA NPs (A) and Berberine-BSA NP formulation (B).

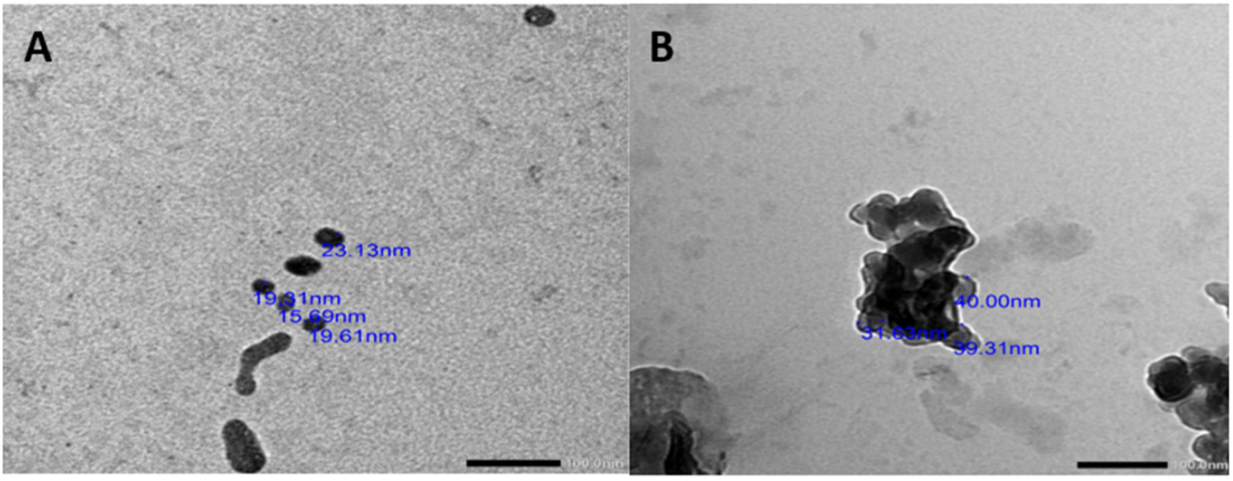

Fig. 4. Transmission electron microscopy (TEM) visualization of BSA and Berberine-BSA nanoparticles. Transmission electron microscopy images of (A) bovine serum albumin nanoparticles (BSA NP) and (B) Berberine-BSA NPs. Scale bar = 100 nm.

(50.4 µmol/mL; $p < 0.001$). Additionally, the DNA fragmentation levels were significantly raised by about 4-fold in treated HepG2 cells in comparison to the untreated control (Table 2; $p < 0.001$).

The statistical analysis results have been conducted using ANOVA. The significance level is set at $p < 0.001$.

Journal of
BIOLOGICAL REGULATORS
and Homeostatic Agents

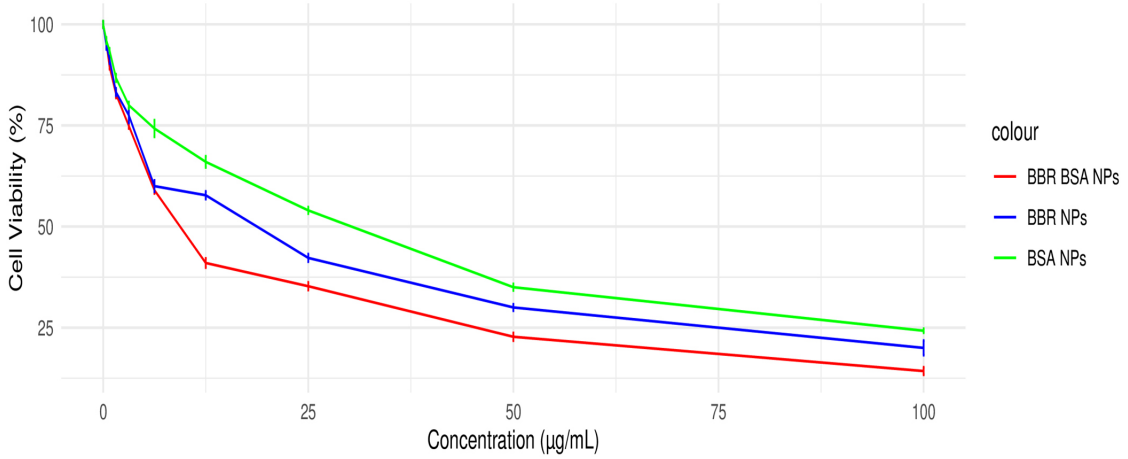

Fig. 5. Effect of various doses of BBR, bovine serum albumin nanoparticles (BSA NPs), and BBR-BSA NPs on HepG2 cell viability. Sample size: n = 3 (triplicates).

Table 2. Lactate dehydrogenase (LDH; U/L), reduced glutathione (GSH) activity (µmol/mL), and caspase-3 level (ng/mL) in treated HepG2 cells after incubation with Berberine (BBR), bovine serum albumin nanoparticles (BSA NPs), and BBR-BSA NPs for 72 h.

Formula	LDH	GSH	Caspase-3	DNA fragmentation
Control	62.4 ± 2.7^{d}	35.2 ± 0.4^{d}	2.01 ± 0.1^{c}	1.7 ± 0.1^{d}
BSA NPs	82.3 ± 1.6^{c}	50.4 ± 0.8^{c}	4.3 ± 0.4^{b}	5.2 ± 0.2^{c}
BBR solution	85.1 ± 1.4^{b}	62.5 ± 0.7^{b}	4.8 ± 0.7^{b}	6.1 ± 0.1^{b}
BBR-BSA NPs	101.7 ± 1.3^{a}	83.1 ± 1.1^{a}	7.03 ± 1.8^{a}	6.9 ± 0.8^{a}
F-value	386.8	3018.6	69.03	132.3
p-value	<0.001	<0.001	<0.001	<0.001

One-way ANOVA and Duncan (Post Hoc analysis) were conducted.
The effect's intensity is categorized alphabetically.
Different letters indicate significant differences, and the same letter signifies nonsignificant differences.

Discussion

Recently, HCC has been shown to have a greater incidence and fatality rate than other kinds of cancer. Patients with HCC are now being treated with a focus on quality-of-life enhancement and survival extension [35]. The BSA NPs have been extensively utilized as drug carriers to deliver chemical and gene pharmaceuticals, considering BSA's exceptional biocompatibility, non-toxicity, and non-immunogenicity [36]. Pharmacokinetic studies have been aiming to ascertain the distribution of the drug's half-life and its capacity to be confined to a specific compartment in the body. This enables targeted treatment delivery to reach desired cells while avoiding entry into other cells or tissues [37]. Generally, the pharmacokinetic properties of BSA NPs can describe their bioavailability. Various drugs possess confined therapeutic efficacy; thus, they are formulated and manufactured as NPs with BSA carriers, increasing drug bioavailability and therapeutic effect [38]. The Chinese herbal medication BBR is an ingredient of *Coptis chinensis*, a well-known drug with various pharmacological properties.

Moreover, BBR is cell type-specific [39], with the ability to elicit various cellular responses in different cells. The anti-tumor potential of BBR has been of considerable interest as an alternative to chemotherapeutic treatment through various pathways [40]. However, BBR is limited to low bioavailability and water solubility; therefore, its delivery to target cells is restricted. Accordingly, to increase the effectiveness of BBR, BSA NPs have been employed as carriers to deliver BBR to the targeted location [30]. The BSA was chosen to preserve the active component BBR from proteolytic degradation and ensure lengthy bloodstream circulation as a delivery vehicle.

Our study computationally investigated the commonly reported targets of BBR through a molecular docking study. The analyzed targets were AKT-1, as BBR was reported to induce human gastric cancer cell apoptosis through modifying the AKT pathway [41]; caspase-3, as BBR was reported to trigger caspase-3 dependent apoptosis in breast cancer cells [42], human leukemia cells [43], human prostate carcinoma cells [44], and human tongue squamous carcinoma [45]. Other analyzed targets also included EGFR, where

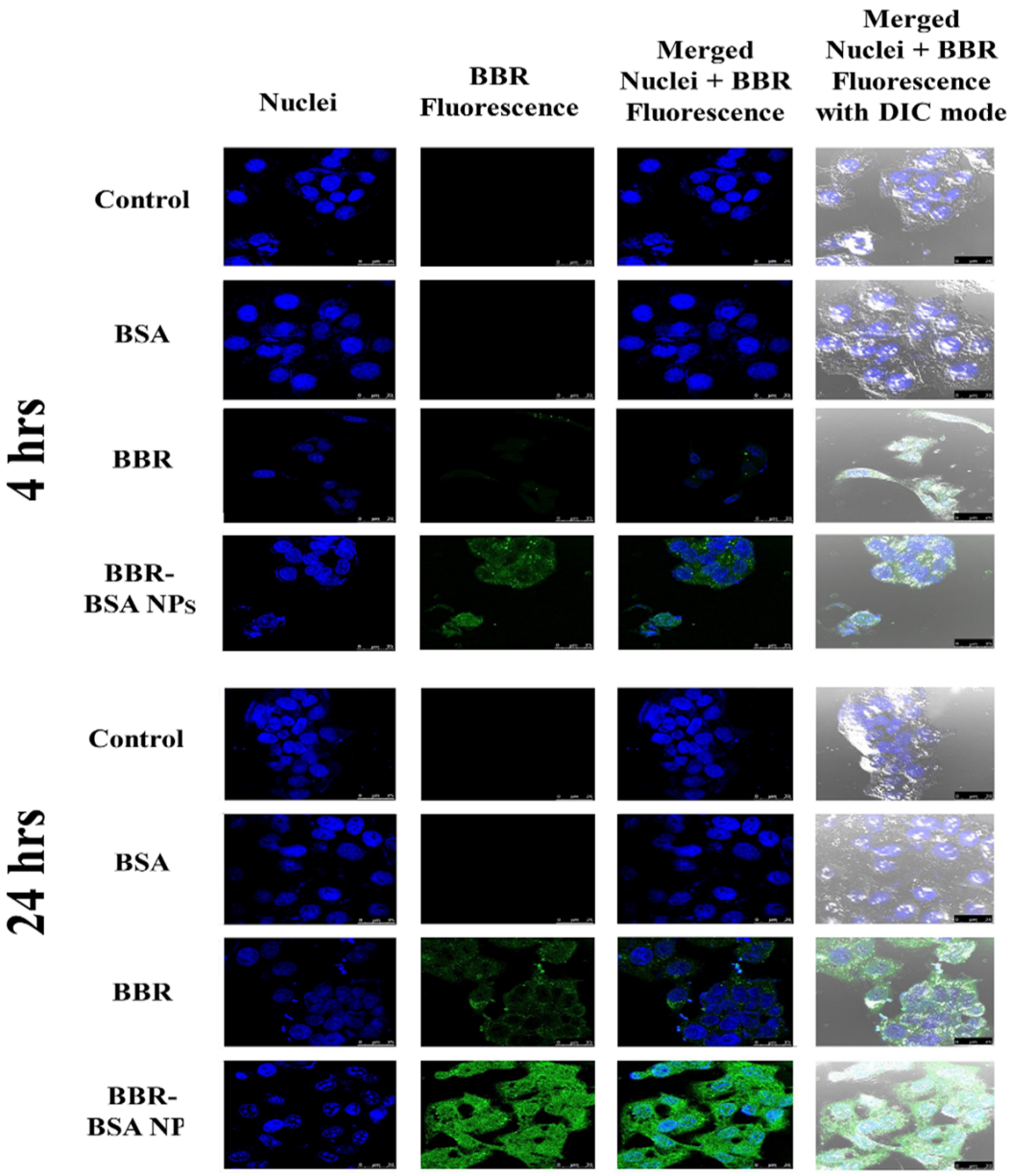

Fig. 6. Confocal microscopy images showing the cellular uptake of BBR, bovine serum albumin nanoparticles (BSA NPs), and BBR-BSA NPs by HepG2 cells after 4 and 24 h compared to the control. Confocal Laser Scanning Microscope × 63, scale bar: 25 µm, scan mode = XYZ Unidirectional X, scan speed = 400 Hz, pinhole diameter = 137.1 µm.

BBR was reported to inhibit EGFR as its anti-tumor activity against gastric cancer [46] and glioblastoma [47]. Docking analyzed targets also comprised ERK-2, which was modified by the action of BBR on pulmonary metastasis [48]; P38, which was activated by the action of BBR on human hepatoma cells [49]; and finally signal transducer and activator of transcription 3 (STAT-3), which was modified by the action of BBR on colorectal cancer cells [50]. The docking study results matched the mentioned mechanisms of BBR as the docking score with each target was close to the control score, suggesting the possibility of BBR as a natural anti-tumor product with multi-target cellular molecules and pathways.

Our study showcased that both BSA NPs and BBR-BSA NPs have nanostructures with a spherical shape with a size of nearly 15.458 ± 1.42 and 36.66 ± 0.97 nm, respectively. This increased size indicates BBR incorporation on the BSA NP surface. This result is consistent with the higher ZP negative charged value of BBR-BSA NPs than BSA NPs, suggesting NPs' good dispersion in aqueous media and the nanosuspensions' strong stability and aggregation tolerance [51]. Herein, the BBR-BSA NPs exhibited a high EE% that is usually desirable for NPs since it enhances their likelihood to transport and release enough drugs to the target location, especially if they are built with a suitably triggered release mechanism and drug release rate.

Journal of
BIOLOGICAL REGULATORS
and Homeostatic Agents

Herein, BBR and BBR-BSA NPs possessed a considerable impact on HepG2 cell viability in a dose-dependent manner consistent with the previously mentioned findings for various cancer cell lines. Furthermore, BBR-BSA NPs exhibited increased cytotoxicity than pure BBR on HepG2 cells at all the concentration levels for 72 h, revealing that BBR-BSA NPs are relatively potent and effective and have higher anti-cancer activities. However, BBR showed higher anti-cancer activity compared with BSA. These findings agreed with Solanki *et al*. [30], who suggested that BBR-BSA NPs exhibited enhanced therapeutic efficacy and BBR anti-cancer properties by facilitating its delivery to the targeted site for future therapeutic applications.

In addition, BBR-BSA NPs were distributed in the cytoplasmic and quiet nuclear regions. The BBR-BSA NPs demonstrated higher cellular uptake efficiency in comparison with BBR, as suggested by the high green fluorescence intensity prominently increased after 24 h incubation, confirming the time-dependent cellular uptake of BSA NPs. The results aligned with the higher BBR-BSA NP cytotoxicity, which may be related to receptor-mediated endocytosis through BSA moieties because of BSA receptor overexpression on the HepG2 cell surface [52–54].

Cell apoptosis is the primary method for most small molecular chemotherapeutic medications to establish if cell apoptosis is essential in inducing cancer cell death and DNA breakage. At varying concentrations, BBR-BSA NPs induced more cell apoptosis than pure BBR; therefore, they appear to have a greater inhibitory or anti-proliferative activity against HepG2 cells than BBR, which confirms the greater efficacy of BBR-BSA NPs in enhancing BBR bioavailability and solubility. Particularly, Hyun *et al*. [41] have concluded that treating HepG2 cells using BBR triggers reactive oxygen species (ROS) generation via Akt phosphorylation, dissociating the ASK1-mediated activation of c-Jun NH2-terminal kinase (JNK) and p38 pathways. Investigating cytokines, receptors, and downstream elements in signaling cascade pathways could confirm these therapeutic effects. These findings show that BBR can trigger cell death through the Fas-mediated [16] suppression of mTOR signaling, besides downregulation of matrix metalloproteinases 9 (MMP 9) expression and the NF-κB and AP-1 pathways. Reduced GSH constitutes a significant non-protein thiol in living creatures; it is essential in coordinating the antioxidant defense processes of the body due to their exposed sulfhydryl groups; non-protein sulfhydryl binds various electrophilic radicals and metabolites that may cause damage to the cells [55]. These findings might be attributed to an increase in the rate of GSH transformation to oxidized glutathione (GSSG) due to GSH consumption to eliminate hydrogen peroxide (H_2O_2) [55]. Overproducing free radicals and ROS would attack key biological components such as DNA, protein, or lipid, leading to numerous degenerative diseases such as cancer [56]. Apoptosis is defined by cell shrinkage, chromatin condensation, internucleosomal DNA fragmentation, and apoptotic body formation. Endogenous ROS can cause cellular DNA damage and stochastic mistakes in replication or recombination, leading to tumor cell death. Our results demonstrated that the high apoptosis rate in cancer cells suggests the release of BBR within these cells, demonstrating the particular anti-cancer effect of the drug. This might be because BBR targets signaling molecules abundant in cancer cells.

Additionally, the significantly increased LDH, caspase-3, GSH, and DNA fragmentation in cells received BSA NP, BBR, or BBR-BSA NP treatment confirm the potential therapeutic effect of BBR. These results were compatible with the findings of Hwang *et al*. [57], who have revealed that BBR might exert a chemopreventive role by decreasing oxidative stress in living systems. Collectively, BBR-BSA NPs provide a biocompatible, non-toxic, and innovative anti-cancer BBR delivery system that can enhance BBR bioavailability in tumor tissues and consequently mediate a more potent anti-cancer effect.

Conclusions

The BBR-BSA NPs have been extensively studied and have shown promising results in our study, demonstrating their ability to accumulate in HepG2 cells and effectively deliver BBR selectively. This targeted delivery system increases the therapeutic efficacy of BBR, making it a safer option for cancer treatment. Furthermore, the innovative nature of the BBR-BSA NPs offers possibilities for further modifications and improvements in drug delivery systems for treating HCC particularly and other malignancies generally.

Availability of Data and Materials

The corresponding author can provide the data upon request.

Author Contributions

GAMK conceptualized the study and designed the research protocol. MAE led the experimental work, handled data analysis, and served as the corresponding author. GAMK contributed to nanoparticle synthesis and characterization. SAD, WKA, and MAA were involved in the molecular docking studies and interpretation of results. TGMA and MSAZ provided expertise in cell culture experiments and viability assays. ANAM assisted with the spectroscopy analysis. AKA contributed to the manuscript preparation, revision and analyzed data. RAE provided critical feedback and helped shape the research, analysis, and manuscript. MAK coordinated the research collaboration, process, funding acquisition and analyzed data. NAM was responsible for statistical analysis and ensured the accuracy of data interpretation. All authors have been involved in revising it critically for important intellectual content. All

authors gave final approval of the version to be published. All authors have participated sufficiently in the work to take public responsibility for appropriate portions of the content and agreed to be accountable for all aspects of the work in ensuring that questions related to its accuracy or integrity.

Ethics Approval and Consent to Participate

Not applicable.

Acknowledgment

We would like to express our gratitude to the Deanship of Scientific Research at King Khalid University for generously funding this work through a large group Research Project (RGP2/40/44). We express our genuine gratitude to EdigenomiX Scientific Co., Ltd for their proficient editing and proofreading services, which significantly enhanced the lucidity and excellence of our article. We greatly applaud their fastidious attention to detail and assistance in revising the paper for publication.

Funding

Funded by the Deanship of Scientific Research at King Khalid University through a large group Research Project (RGP2/40/44).

Conflict of Interest

The authors declare no conflict of interest.

References

[1] Sung H, Ferlay J, Siegel RL, Laversanne M, Soerjomataram I, Jemal A, *et al*. Global Cancer Statistics 2020: GLOBOCAN Estimates of Incidence and Mortality Worldwide for 36 Cancers in 185 Countries. CA: a Cancer Journal for Clinicians. 2021; 71: 209–249.

[2] Ye Y, Liu X, Wu N, Han Y, Wang J, Yu Y, *et al*. Efficacy and Safety of Berberine Alone for Several Metabolic Disorders: A Systematic Review and Meta-Analysis of Randomized Clinical Trials. Frontiers in Pharmacology. 2021; 12: 653887.

[3] Remppis A, Bea F, Greten HJ, Buttler A, Wang H, Zhou Q, *et al*. Rhizoma Coptidis inhibits LPS-induced MCP-1/CCL2 production in murine macrophages via an AP-1 and NFkappaB-dependent pathway. Mediators of Inflammation. 2010; 2010: 194896.

[4] Zhang J, Song J, Li H, Li Z, Chen M, Ma S, *et al*. Berberine protects against neomycin-induced ototoxicity by reducing ROS generation and activating the PI3K/AKT pathway. Neuroscience Letters. 2023; 817: 137518.

[5] Sun J, Bao H, Peng Y, Zhang H, Sun Y, Qi J, *et al*. Improvement of intestinal transport, absorption and anti-diabetic efficacy of berberine by using Gelucire44/14: In vitro, in situ and in vivo studies. International Journal of Pharmaceutics. 2018; 544: 46–54.

[6] Feng X, Sureda A, Jafari S, Memariani Z, Tewari D, Annunziata G, *et al*. Berberine in Cardiovascular and Metabolic Diseases: From Mechanisms to Therapeutics. Theranostics. 2019; 9: 1923–1951.

[7] Zhan Y, Han J, Xia J, Wang X. Berberine Suppresses Mice Depression Behaviors and Promotes Hippocampal Neurons Growth Through Regulating the miR-34b-5p/miR-470-5p/BDNF Axis. Neuropsychiatric Disease and Treatment. 2021; 17: 613–626.

[8] Zhang Y, Wang X, Sha S, Liang S, Zhao L, Liu L, *et al*. Berberine increases the expression of NHE3 and AQP4 in sennosideA-induced diarrhoea model. Fitoterapia. 2012; 83: 1014–1022.

[9] Zhang L, Chang JJ, Zhang SL, Damu GLV, Geng RX, Zhou CH. Synthesis and bioactive evaluation of novel hybrids of metronidazole and berberine as new type of antimicrobial agents and their transportation behavior by human serum albumin. Bioorganic & Medicinal Chemistry. 2013; 21: 4158–4169.

[10] Kulkarni SK, Dhir A. Berberine: a plant alkaloid with therapeutic potential for central nervous system disorders. Phytotherapy Research. 2010; 24: 317–324.

[11] Zhao Z, Wei Q, Hua W, Liu Y, Liu X, Zhu Y. Hepatoprotective effects of berberine on acetaminophen-induced hepatotoxicity in mice. Biomedicine & Pharmacotherapy. 2018; 103: 1319–1326.

[12] Yu P, Li D, Ni J, Zhao L, Ding G, Wang Z, *et al*. Predictive QSAR modeling study on berberine derivatives with hypolipidemic activity. Chemical Biology & Drug Design. 2018; 91: 867–873.

[13] Kou Y, Tong B, Wu W, Liao X, Zhao M. Berberine Improves Chemo-Sensitivity to Cisplatin by Enhancing Cell Apoptosis and Repressing PI3K/AKT/mTOR Signaling Pathway in Gastric Cancer. Frontiers in Pharmacology. 2020; 11: 616251.

[14] Rauf A, Abu-Izneid T, Khalil AA, Imran M, Shah ZA, Emran TB, *et al*. Berberine as a Potential Anticancer Agent: A Comprehensive Review. Molecules. 2021; 26: 7368.

[15] Kuo HP, Chuang TC, Yeh MH, Hsu SC, Way TD, Chen PY, *et al*. Growth suppression of HER2-overexpressing breast cancer cells by berberine via modulation of the HER2/PI3K/Akt signaling pathway. Journal of Agricultural and Food Chemistry. 2011; 59: 8216–8224.

[16] Kim JS, Oh D, Yim MJ, Park JJ, Kang KR, Cho IA, *et al*. Berberine induces FasL-related apoptosis through p38 activation in KB human oral cancer cells. Oncology Reports. 2015; 33: 1775–1782.

[17] Kim S, Han J, Lee SK, Choi MY, Kim J, Lee J, *et al*. Berberine suppresses the TPA-induced MMP-1 and MMP-9 expressions through the inhibition of PKC-α in breast cancer cells. The Journal of Surgical Research. 2012; 176: e21–e29.

[18] Mirhadi E, Rezaee M, Malaekeh-Nikouei B. Nano strategies for berberine delivery, a natural alkaloid of Berberis. Biomedicine & Pharmacotherapy. 2018; 104: 465–473.

[19] Kratz F. Albumin as a drug carrier: design of prodrugs, drug conjugates and nanoparticles. Journal of Controlled Release. 2008; 132: 171–183.

[20] Zhang Y, Sun T, Jiang C. Biomacromolecules as carriers in drug delivery and tissue engineering. Acta Pharmaceutica Sinica. B. 2018; 8: 34–50.

[21] Zhang X, He Q, Cui Y, Duan L, Li J. Human serum albumin supported lipid patterns for the targeted recognition of microspheres coated by membrane based on ss-DNA hybridization. Biochemical and Biophysical Research Communications. 2006; 349: 920–924.

[22] An Z, Lu G, Möhwald H, Li J. Self-assembly of human serum albumin (HSA) and L-alpha-dimyristoylphosphatidic acid (DMPA) microcapsules for controlled drug release. Chemistry. 2004; 10: 5848–5852.

[23] Yang Z, Zhang N, Ma T, Liu L, Zhao L, Xie H. Engineered bovine serum albumin-based nanoparticles with pH-sensitivity for doxorubicin delivery and controlled release. Drug Delivery. 2020; 27: 1156–1164.

[24] Patel S, Datta A. Steady state and time-resolved fluorescence

investigation of the specific binding of two chlorin derivatives with human serum albumin. The Journal of Physical Chemistry. B. 2007; 111: 10557–10562.

[25] Guo P, Cai C, Wu X, Fan X, Huang W, Zhou J, *et al*. An Insight Into the Molecular Mechanism of Berberine Towards Multiple Cancer Types Through Systems Pharmacology. Frontiers in Pharmacology. 2019; 10: 857.

[26] Ai X, Yu P, Peng L, Luo L, Liu J, Li S, *et al*. Berberine: A Review of its Pharmacokinetics Properties and Therapeutic Potentials in Diverse Vascular Diseases. Frontiers in Pharmacology. 2021; 12: 762654.

[27] Song D, Hao J, Fan D. Biological properties and clinical applications of berberine. Frontiers of Medicine. 2020; 14: 564–582.

[28] Trott O, Olson AJ. AutoDock Vina: improving the speed and accuracy of docking with a new scoring function, efficient optimization, and multithreading. Journal of Computational Chemistry. 2010; 31: 455–461.

[29] Seeliger D, de Groot BL. Ligand docking and binding site analysis with PyMOL and Autodock/Vina. Journal of Computer-Aided Molecular Design. 2010; 24: 417–422.

[30] Solanki R, Patel K, Patel S. Bovine Serum Albumin Nanoparticles for the Efficient Delivery of Berberine: Preparation, Characterization and In vitro biological studies. Colloids and Surfaces A: Physicochemical and Engineering Aspects. 2021; 608: 125501.

[31] Nicholson DW, Thornberry NA. Caspases: killer proteases. Trends in Biochemical Sciences. 1997; 22: 299–306.

[32] Beutler E, Duron O, Kelly BM. Improved method for the determination of blood glutathione. The Journal of Laboratory and Clinical Medicine. 1963; 61: 882–888.

[33] Rahbar Saadat Y, Saeidi N, Zununi Vahed S, Barzegari A, Barar J. An update to DNA ladder assay for apoptosis detection. BioImpacts. 2015; 5: 25–28.

[34] Itoh G, Tamura J, Suzuki M, Suzuki Y, Ikeda H, Koike M, *et al*. DNA fragmentation of human infarcted myocardial cells demonstrated by the nick end labeling method and DNA agarose gel electrophoresis. The American Journal of Pathology. 1995; 146: 1325–1331.

[35] Gandhi S, Khubchandani S, Iyer R. Quality of life and hepatocellular carcinoma. Journal of Gastrointestinal Oncology. 2014; 5: 296–317.

[36] Loureiro A, Azoia NG, Gomes AC, Cavaco-Paulo A. Albumin-Based Nanodevices as Drug Carriers. Current Pharmaceutical Design. 2016; 22: 1371–1390.

[37] Hashida M. Role of pharmacokinetic consideration for the development of drug delivery systems: A historical overview. Advanced Drug Delivery Reviews. 2020; 157: 71–82.

[38] Huang Y, Deng S, Luo X, Liu Y, Xu W, Pan J, *et al*. Evaluation of Intestinal Absorption Mechanism and Pharmacokinetics of Curcumin-Loaded Galactosylated Albumin Nanoparticles. International Journal of Nanomedicine. 2019; 14: 9721–9730.

[39] Li CL, Tan LH, Wang YF, Luo CD, Chen HB, Lu Q, *et al*. Comparison of anti-inflammatory effects of berberine, and its natural oxidative and reduced derivatives from Rhizoma Coptidis in vitro and in vivo. Phytomedicine. 2019; 52: 272–283.

[40] Dong Y, Chen H, Gao J, Liu Y, Li J, Wang J. Bioactive Ingredients in Chinese Herbal Medicines That Target Non-coding RNAs: Promising New Choices for Disease Treatment. Frontiers in Pharmacology. 2019; 10: 515.

[41] Hyun MS, Hur JM, Mun YJ, Kim D, Woo WH. BBR induces apoptosis in HepG2 cell through an Akt-ASK1-ROS-p38MAPKs-linked cascade. Journal of Cellular Biochemistry. 2010; 109: 329–338.

[42] Zhao Y, Jing Z, Li Y, Mao W. Berberine in combination with cisplatin suppresses breast cancer cell growth through induction of DNA breaks and caspase-3-dependent apoptosis. Oncology Reports. 2016; 36: 567–572.

[43] Okubo S, Uto T, Goto A, Tanaka H, Nishioku T, Yamada K, *et al*. Berberine Induces Apoptotic Cell Death via Activation of Caspase-3 and -8 in HL-60 Human Leukemia Cells: Nuclear Localization and Structure-Activity Relationships. The American Journal of Chinese Medicine. 2017; 45: 1497–1511.

[44] Mantena SK, Sharma SD, Katiyar SK. Berberine, a natural product, induces G1-phase cell cycle arrest and caspase-3-dependent apoptosis in human prostate carcinoma cells. Molecular Cancer Therapeutics. 2006; 5: 296–308.

[45] Ho YT, Lu CC, Yang JS, Chiang JH, Li TC, Ip SW, *et al*. Berberine induced apoptosis via promoting the expression of caspase-8, -9 and -3, apoptosis-inducing factor and endonuclease G in SCC-4 human tongue squamous carcinoma cancer cells. Anticancer Research. 2009; 29: 4063–4070.

[46] Wang J, Yang S, Cai X, Dong J, Chen Z, Wang R, *et al*. Berberine inhibits EGFR signaling and enhances the antitumor effects of EGFR inhibitors in gastric cancer. Oncotarget. 2016; 7: 76076–76086.

[47] Liu Q, Xu X, Zhao M, Wei Z, Li X, Zhang X, *et al*. Berberine induces senescence of human glioblastoma cells by downregulating the EGFR-MEK-ERK signaling pathway. Molecular Cancer Therapeutics. 2015; 14: 355–363.

[48] Hamsa TP, Kuttan G. Berberine inhibits pulmonary metastasis through down-regulation of MMP in metastatic B16F-10 melanoma cells. Phytotherapy Research. 2012; 26: 568–578.

[49] Hur JM, Hyun MS, Lim SY, Lee WY, Kim D. The combination of berberine and irradiation enhances anti-cancer effects via activation of p38 MAPK pathway and ROS generation in human hepatoma cells. Journal of Cellular Biochemistry. 2009; 107: 955–964.

[50] Liu X, Ji Q, Ye N, Sui H, Zhou L, Zhu H, *et al*. Berberine Inhibits Invasion and Metastasis of Colorectal Cancer Cells via COX-2/PGE2 Mediated JAK2/STAT3 Signaling Pathway. PLoS ONE. 2015; 10: e0123478.

[51] Imam SS, Alshehri S, Ghoneim MM, Zafar A, Alsaidan OA, Alruwaili NK, *et al*. Recent Advancement in Chitosan-Based Nanoparticles for Improved Oral Bioavailability and Bioactivity of Phytochemicals: Challenges and Perspectives. Polymers. 2021; 13: 4036.

[52] Varshosaz J, Farzan M. Nanoparticles for targeted delivery of therapeutics and small interfering RNAs in hepatocellular carcinoma. World Journal of Gastroenterology. 2015; 21: 12022–12041.

[53] Li M, Zhang W, Wang B, Gao Y, Song Z, Zheng QC. Ligand-based targeted therapy: a novel strategy for hepatocellular carcinoma. International Journal of Nanomedicine. 2016; 11: 5645–5669.

[54] Huang Y, Hu L, Huang S, Xu W, Wan J, Wang D, *et al*. Curcumin-loaded galactosylated BSA nanoparticles as targeted drug delivery carriers inhibit hepatocellular carcinoma cell proliferation and migration. International Journal of Nanomedicine. 2018; 13: 8309–8323.

[55] Szabo S, Nagy L, Plebani M. Glutathione, protein sulfhydryls and cysteine proteases in gastric mucosal injury and protection. Clinica Chimica Acta. 1992; 206: 95–105.

[56] Fang YZ, Yang S, Wu G. Free radicals, antioxidants, and nutrition. Nutrition. 2002; 18: 872–879.

[57] Hwang JM, Wang CJ, Chou FP, Tseng TH, Hsieh YS, Lin WL, *et al*. Inhibitory effect of berberine on tert-butyl hydroperoxide-induced oxidative damage in rat liver. Archives of Toxicology. 2002; 76: 664–670.